Environmental Science and Ecotechnology 28 (2025) 100630

Contents lists available at ScienceDirect

Environmental Science and Ecotechnology

journal homepage: www.journals.elsevier.com/environmental-science-and-ecotechnology/

Original Research

Chaperone-mediated thermotolerance in hyperthermophilic composting: Molecular-Level protein remodeling of microbial communities

Xu Li [a], Youzhao Wang [a], Feng Ma [b], Chaoyue Zhao [a], Yanping Zhang [a], Yaonan Zhu [c], Yang Zhang [d], Shujie Hou [a], Bingzhen Li [a], Fuxin Yang [a], Liying Hao [e,*], Tong Zhu [a,**]

[a] Institute of Process Equipment and Environmental Engineering, School of Mechanical Engineering and Automation, Northeastern University, Shenyang, 110819, China
[b] School of Environment and Resources, Taiyuan University of Science and Technology, Taiyuan, 030024, China
[c] School of Engineering, The University of Tokyo, Tokyo, 113-8656, Japan
[d] School of Public Health, China Medical University, Shenyang, 110122, China
[e] Department of Pharmaceutical Toxicology, School of Pharmacy, China Medical University, Shenyang, 110122, China

ARTICLE INFO

Article history:
Received 24 March 2025
Received in revised form
19 October 2025
Accepted 20 October 2025

Keywords:
Hyperthermophilic composting
Metabolism function
Heat-shock proteins
Heat-resistant mechanism
Molecular dynamics

ABSTRACT

Hyperthermophilic composting (HC) represents a promising approach for converting organic solid waste into valuable resources by leveraging extreme temperatures to enhance microbial degradation and detoxification processes. In this high-temperature environment, microbial communities undergo dynamic succession, where thermophilic bacteria dominate and drive efficient organic matter transformation through adapted metabolic pathways and stress responses. These adaptations include the stabilization of cellular structures and enzymes, often mediated by heat shock proteins (HSPs) that prevent protein misfolding under thermal stress. However, the integrated mechanisms linking community-level functional shifts to molecular-level protein remodeling in thermophiles during HC remain poorly understood. Here we show a coordinated interaction of functional succession and molecular adaptations within thermophilic bacteria in HC, which collectively achieve heat resistance. This interaction encompasses enhanced metabolic and genetic modules, accounting for 97% of the variance observed in thermophile abundance. Metagenomic analyses revealed upregulation of translation, transcription, amino acid metabolism, and cell wall biosynthesis, coupled with suppression of mobilome functions to maintain genomic stability, as confirmed by partial least squares path modeling and Boruta analyses. Molecular dynamics simulations of key enzymes from the thermophile *Truepera* further demonstrated intrinsic structural rigidity, reduced hydrophobic exposure, and hierarchical chaperone activity involving DNAJ, DNAK, and GroEL for protein repair. These findings enhance our comprehension of microbial thermotolerance and establish a foundation for optimizing composting efficiency and advancing heat-resistant microbial applications in biotechnology and waste management. Additionally, they offer insights into the evolution of thermophiles, protein engineering, and stress adaptation across various biological and industrial systems, thereby promoting the integration of environmental engineering and systems biology.

1. Introduction

In the face of escalating global environmental challenges, hyperthermophilic composting (HC)—with its extreme temperature (>80 °C) environment and high-efficiency humification characteristics—demonstrates revolutionary potential in the field of organic solid waste resource utilization. The core process of HC

* Corresponding author.
** Corresponding author.
E-mail addresses: lyhao@cmu.edu.cn (L. Hao), tongzhu@mail.neu.edu.cn (T. Zhu).

https://doi.org/10.1016/j.ese.2025.100630

involves three dynamic balances: the dynamic succession of thermophilic microbial communities, the degradation and transformation of organic matter, and thermally driven gas–liquid–solid mass transfer processes. Notably, the formation of a three-dimensional (3D) gradient field of temperature, oxygen concentration, and moisture within the compost heap establishes a dynamic ecological environment for microorganisms with varying heat resistance. This environment not only selects for unique hyperthermophiles strains but also drives microorganisms to evolve complex regulatory mechanisms for thermotolerance. Thermophiles, primarily bacteria and archaea capable of thriving at elevated temperatures (>55 °C), have been extensively isolated from extreme environments, such as compost heaps, hot springs, volcanoes, and geothermal habitats [1]. They exhibit a wide array of industrial applications, including biopharmaceutical production [2,3], genetic engineering [4–7], and biochemicals synthesis [8–10]. Oshima and Moriya first demonstrated the feasibility of inoculating thermophiles into compost systems to achieve temperatures exceeding 100 °C, markedly surpassing conventional composting peaks of approximately 65–70 °C [11]. Compared to traditional composting methods, HC facilitates more efficient organic matter degradation, significantly shortens processing time, enhances humification [12], and accelerates the removal of pathogens, toxic metals, and antibiotics [13–15].

During the HC process, thermophiles activate several thermotolerance mechanisms involving multiple complex biological processes, primarily including adaptation of cell membranes, protein stabilization, and maintenance of metabolic enzyme function. Studies have revealed that the membranes of thermophiles—especially hyperthermophiles—are enriched with saturated fatty acids and specific lipid molecules—such as diethyl and tetraethers—which confer structural stability at extreme temperatures [16]. Moreover, thermophiles can synthesize large quantities of heat shock proteins (HSPs), such as HSP70 and HSP60, in response to heat stress. These proteins play a protective role in cellular stress responses by preventing protein denaturation and aggregation [17–19]. In addition to membrane and protein stability, the enzyme systems of thermophiles also exhibit a high degree of thermostability [9,20–22]. The catalytic efficiency of these thermotolerant enzymes is maintained at elevated temperatures and is widely utilized in biotechnology, such as for the industrial production of cellulases and amylases [23–25]. However, existing research has predominantly focused on the thermotolerance characteristics of single strains under laboratory conditions, and studies on the functional differentiation and cooperative mechanisms of thermophiles and hyperthermophiles in complex real-world environments remain limited. Specifically, the unique heat adaptation strategies of these thermophilic microorganisms in composting environments—including the synergistic repair mechanism of misfolded proteins by HSPs and the thermotolerance regulatory network of metabolic functions under heat stress—have not yet been systematically analyzed. Given the tremendous potential of HC to transform organic solid waste into a valuable resource and to facilitate its harmless disposal, an in-depth investigation into the heat resistance mechanisms of thermophiles and hyperthermophiles during composting is essential. Such research will elucidate their survival strategies in highly complex and dynamic environments, providing a scientific foundation and technical support for optimizing composting processes, harnessing thermophilic microbial resources, and advancing their conversion into bioenergy.

This study aims to bridge this research gap by providing new insights into the evolution and synergy of microbial heat resistance mechanisms during HC, thereby offering a solid theoretical foundation for optimizing HC processes and improving the efficiency of organic waste degradation. The specific objectives are: (1) to clarify the metabolic pathways of thermophiles in HC; (2) to explore the potential mechanisms affecting the thermal stability of thermophiles and hyperthermophiles; (3) to uncover the physiological adaptability and heat resistance molecular mechanisms of key enzymes in thermophiles under high-temperature conditions; and (4) to analyze the 3D structures of HSP–substrate protein complexes at high temperatures, locate key thermostable structural domain allosteric regulatory sites, and further verify their molecular conformations and functional stability under heat stress.

2. Materials and methods

2.1. Hyperthermophilic composting devices and materials

To achieve the stated objectives, we employed a semi-automated intelligent aerobic composting device consisting of a composting reactor, a temperature and moisture content detector (Campbell, CS650, Logan, Utah, USA), an aeration system (Jieba, XGB-120, Dongguan, China), and an intelligent control and feedback system. The composting reactor had a capacity of 1 m^3 and was equipped with ventilation and drainage pipes at the base, enabling an airflow rate of 1.2 m^3 h^{-1}. The reactor exterior was insulated to minimize heat loss. Real-time data on temperature and water content were collected by a data acquisition module (Yanhua, USB-5820, Kunshan, China) and transmitted to a host computer. The composting feedstock consisted primarily of chicken manure (200 kg), agricultural waste (including corn stalks, rice bran, and wheat bran, 100 kg), all sourced from a farm in Shenyang, Liaoning Province, China. The initial moisture contents of the raw materials were 74.3% for chicken manure and 12.3% for the agricultural waste. The microbial agents (containing thermophilic bacteria such as *Calditerricola* and *Thermaerobacter*; 20 kg) were provided by Northeastern University in China, and decomposed products from a previous composting cycle were used as auxiliary materials (60 kg) to enhance the efficiency of the composting process [12,14].

2.2. Experimental procedure and HC sample collection

The raw materials were thoroughly mixed with 20 kg of water and loaded into the composting reactor, which was connected to the temperature and moisture content detection devices, as well as to the aeration system (Fig. 1a). The experiment was conducted in three groups, with the results averaged for analysis, each group employed identical experimental conditions and procedures to validate the reliability and stability of the results. Turning and sampling were performed on Days 0, 3, 6, 9, 12, 15, 18, and 24. At each time point, we collected three samples per group, each composed of five subsamples taken from the corners and center of the heap to minimize spatial heterogeneity. These samples were treated as independent biological replicates. All samples were stored at −80 °C for subsequent physicochemical analysis and high-throughput sequencing. Real-time changes in temperature and water content were continuously recorded. Total organic carbon (TOC) and total nitrogen (TN) contents were measured using a TOC analyzer (HACH, QL3550, Shanghai, China) and a nitrogen monitor (HACH, NT6800, Shanghai, China). We determined ammonia, nitrate, and nitrite nitrogen levels by a triple nitrogen meter (Lianhua, LH-NC3M, Beijing, China). Based on temperature dynamics and humification index (HI—humic acid (HA) to fulvic acid (FA) ratio), the composting process was divided into three phases: the initial phase (IP; Day 0), the thermophilic phase (TP; Days 1–12, average temperature >70 °C), and the maturation phase (MP; Days 13–24, HI > 2.0). Samples were collected at each phase and subjected to metagenomic sequencing to cover the entire

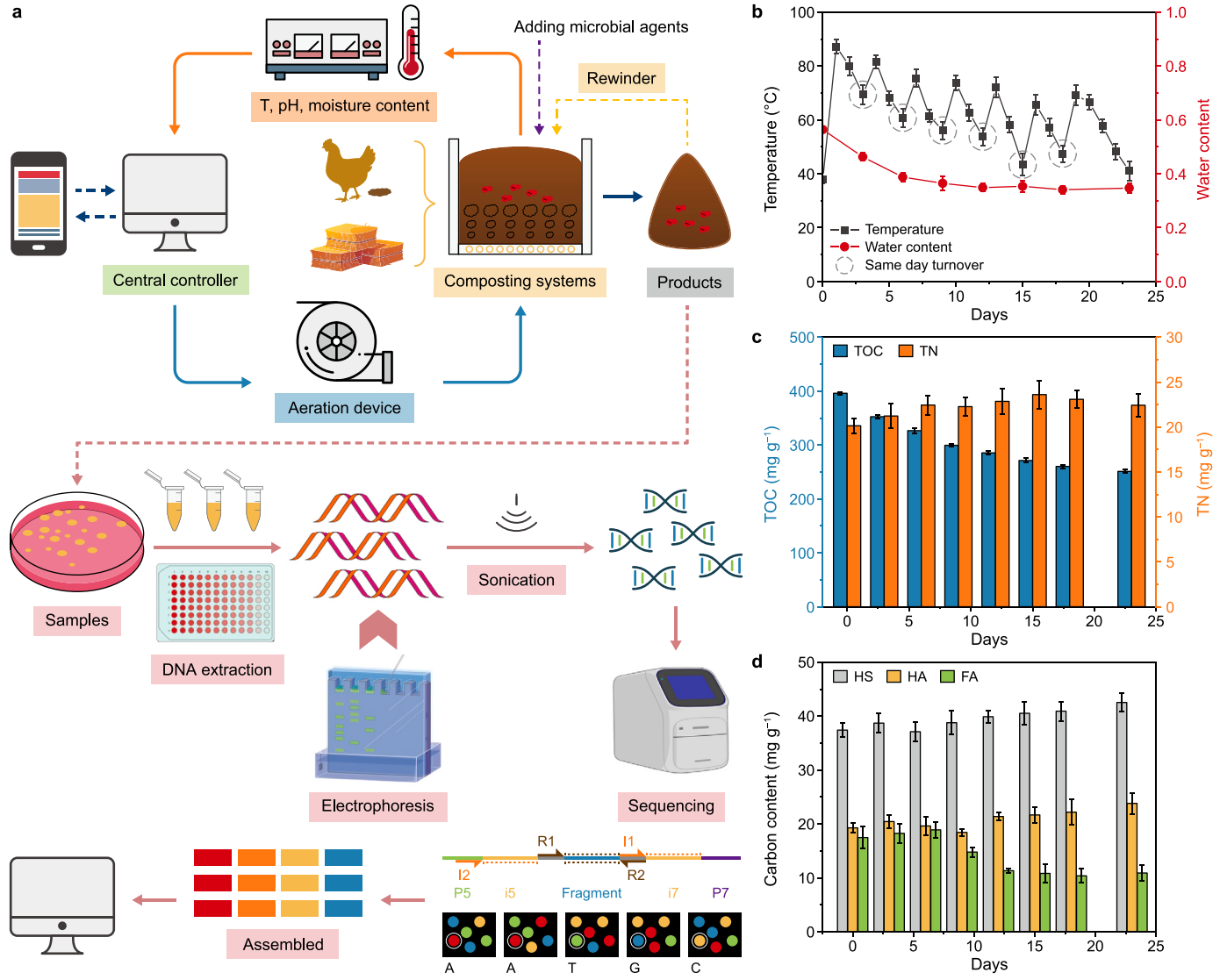

Fig. 1. Composting workflow and physicochemical dynamics. a, Schematic of the intelligent monitoring and control system for composting process automation. T: temperature. **b**, Temporal profiles of temperature and moisture content during hyperthermophilic composting. Error bars represent standard error ($n = 3$ biological replicates). Circular markers indicate turning events for oxygen replenishment and homogeneous fermentation. **c**, Evolution of total organic carbon (TOC) and total nitrogen (TN) during composting. **d**, Dynamic changes in carbon content within humic substances. HS: humic substances; HA: humic acid; FA: fulvic acid.

process of physical and chemical changes and the microbial community succession.

2.3. DNA extraction and detection

Total DNA was extracted from the compost samples using the FastDNA® Spin Kit for Soil DNA Extraction (MP Biomedicals, USA). The integrity of the genomic DNA was assessed using 1% agarose gel electrophoresis, and the DNA concentration and purity were measured with a NanoDrop2000 spectrophotometer (Thermo Scientific, USA). The DNA was then fragmented to approximately 350 bp using an ultrasonic processor (Covaris M220, Woburn, USA). Then, a DNA library was constructed using the NEXTFLEX Rapid DNA-Seq Kit (Bluescape Scientific, Beijing, China).

2.4. Metagenomic sequencing

Metagenomic sequencing was performed using the Illumina NovaSeq X Plus sequencing platform (Shanghai Majorbio Biopharm Technology Co., Ltd, China). Initially, the amplified template molecules were immobilized on a chip, where dense DNA clusters were formed and then linearized into single strands through bridge amplification. Modified DNA polymerase and fluorescently labeled deoxy-ribonucleoside triphosphates (dNTPs) were subsequently added to synthesize one base per reaction cycle. The fluorescent signals produced during the synthesis were recorded via laser scanning to identify the nucleotide species. After several cycles, the “fluorescent group” and the “termination group” were cleaved, restoring the 3’ end adhesion and enabling the decoding of the template DNA sequence.

2.5. Metagenomic data quality control and assembly

We conducted quality control of the sequencing data using the software fastp (version 0.20.0, USA, https://github.com/OpenGene/fastp) [26]. Adapter sequences were trimmed from

both the 3′ and 5' ends, and reads were discarded if they were shorter than 50 bp, had an average base quality score below 20, or contained N bases. We retained high-quality paired-end reads, along with single-end reads, for further analysis. The remaining data were assembled using the software megahit (version 1.1.2, USA, https://github.com/voutcn/megahit) [27], following the principle of succinct de Bruijn graphs. From the assembly, contigs of ≥300 bp were selected as the final output. Open reading frame prediction was performed for the assembled contigs using the software Prodigal (version 2.6.3, USA, https://github.com/hyattpd/Prodigal) [28]. Genes with a nucleic acid length of ≥100 bp were translated into amino acid sequences. The predicted gene sequences from all samples were clustered using the software CD-HIT (Cluster Database at High Identity with Tolerance, version 4.6.1, USA) [29] at 90% identity and 90% coverage. The longest sequences in each cluster were selected as representative sequences to form a nonredundant gene set. High-quality reads from each sample were then aligned to the nonredundant gene set using SOAPaligner (Short Oligonucleotide Analysis Package, version 2.21, China) [30] at a 95% identity threshold, and gene abundance was calculated accordingly. To gain insights into the taxonomic and functional characteristics, amino acid sequences of the nonredundant gene set were compared against the Non-Redundant Protein Database (NR), Kyoto Encyclopedia of Genes and Genomes (KEGG), and other databases using the Diamond software (version 0.8.35, USA) [31]. The BLASTP expectation *e*-value was set to 1×10^{-5}. Relative species and functional abundances were then derived from normalized gene abundance values.

2.6. Molecular dynamics simulation of Truepera radiovictrix key enzyme under thermal stimulation

To investigate the thermal stability of key enzymes in the thermophile *Truepera radiovictrix* (*T. radiovictrix*) during HC, we retrieved target protein structures from the Uniprot database. Classical molecular dynamics (MD) simulations were performed using the software GROMACS 2020 (the Netherlands) [32,33], with the AMBER99SB-ILDN force field and the spc216 three-point water model to accurately describe the protein's secondary structure and side-chain interactions at high temperatures. The protein was placed in a cubic or orthorhombic box with a minimum 1.0 nm buffer from the box boundary. Na^+ or Cl^- ions were added to neutralize the system and maintain physiological ionic strength. Energy minimization was conducted using the steepest descent algorithm, followed by number of particles, volume, temperature (NVT) equilibration with a modified Berendsen thermostat, and number of particles, pressure, temperature (NPT) equilibration using Parrinello–Rahman pressure coupling to stabilize pressure at 1 bar. After releasing positional restraints, the v-rescale thermostat was applied to maintain the temperature at 360 K. Simulation runs consisted of 100 ns simulations with a 2 fs timestep, employing the LINCS algorithm to constrain hydrogen bonds and ensure conformational convergence and achieve dynamic equilibrium. To ensure reliability, we conducted three independent parallel simulations. Post-simulation, trajectories were corrected for periodic boundary effects, and indicators—including the root mean square deviation (RMSD), root mean square fluctuation (RMSF), radius of gyration (Rg), and solvent-accessible surface area (SASA)—were analyzed to evaluate conformational stability, hydrogen-bonding networks, and protein compactness. Additionally, free energy landscape analysis was employed to identify global folding barriers and the distribution of metastable conformations, thereby uncovering the intrinsic thermotolerance and chaperone-assisted mechanisms that enable thermophiles to survive under extreme composting conditions.

2.7. Chaperone–protein docking

To investigate the intracellular chaperone-synergistic mechanisms in thermophiles during HC, chaperone–protein docking was conducted using the software HADDOCK 2.4 [34,35]. This platform integrates nuclear magnetic resonance (NMR) chemical shift perturbation data to refine active-site definitions and improve docking accuracy. Protein structures derived from molecular dynamics simulations were used as receptors, and heat shock proteins (HSPs; e.g., *dnaK* and *dnaJ*) as ligands. Preprocessing removed nonessential molecules (water, Na^+, Cl^-), rebuilt missing atoms, and defined active and passive residues. Active residues were identified based on NMR chemical shift perturbation data and relevant literature, while passive residues were defined as regions adjacent to the active site, enhancing the biological relevance of the docking. The docking process followed a multistage optimization strategy, comprising rigid-body docking, semiflexible refinement of the interfacial region, and hydrate refinement in an explicit aqueous environment to generate high-quality complex models. Candidate models were screened using scoring functions and cluster analysis, and representative structures were selected for further mechanistic studies. Binding interfaces and interaction patterns between the intracellular HSPs (e.g., *dnaK* and *dnaJ*) and the target proteins were visualized using the PyMOL software (USA), providing a critical structural foundation for understanding the molecular mechanisms of chaperone synergy in HC.

2.8. Statistical analysis

All experiments were conducted with triplicate biological replicates ($n = 3$). We visualized data using the software tools Origin 2021 and R Studio (v4.4.2, USA), and performed statistical analyses in Prism 10.4.2 (GraphPad Software, USA). Differential KEGG metabolic pathways were visualized using volcano plots generated with the *DESeq2* package in R. Beta diversity was assessed via principal coordinates analysis, implemented using the *vegan* package in R. Microbial co-occurrence networks were constructed and visualized in Gephi (v0.9.2, France). We used *ggcor* package in R to perform the Mantel tests ($P < 0.05$) to evaluate correlations between the abundance of dominant thermophiles and associated metabolic functions. To elucidate variable interactions in thermotolerance mechanisms, we applied partial least squares path modeling (PLS–PM) using the *plspm* package, and quantified variable importance with the random forest-based Boruta algorithm, implemented via the *Boruta* package in R.

3. Results and discussion

3.1. Physicochemical properties and metabolic functional succession of microbial communities during HC

This study highlights the significant advantages of HC in accelerating humification and improving the efficiency of organic matter transformation. The pile temperature rapidly peaked at 87 °C within 24 h (Fig. 1b), surpassing the 70 °C threshold commonly used to define HC in current research and practice [13,36–38]. The moisture content steadily decreased from 55% to 37%, indicating efficient water evaporation and the vigorous metabolic activity of extreme thermophiles, which is consistent with the characteristics of HC [12]. During the TP, the daily TOC degradation rate reached 3.7%, while TN retention increased by 17.2% (Fig. 1c). This phenomenon can be attributed to the mass concentration effect and microbial immobilization unique to HC, highlighting its effectiveness in mitigating carbon loss and conserving nitrogen. Meanwhile, these extreme conditions not

only accelerated pathogen inactivation but also significantly enhanced humus synthesis [39]. Both the humic substances (HS) and HA contents increased significantly, with HS increasing by 6.1 mg L^{-1} from the initial level and the HA/FA ratio reaching 2.1 (Fig. 1d), suggesting the conversion of HA into more stable HS and improved humus maturity and stability.

The tight coupling between these physicochemical properties and temperature variations is primarily driven by microbial communities and their functional traits. To elucidate this linkage, we employed metagenomic sequencing to characterize microbial communities and functional profiles across distinct composting phases—IP, TP, and MP. The phyla Bacteroidota and Bacillota were dominant during the IP (29.8% and 25.4%, respectively; Fig. 2a), primarily consisting of anaerobic or facultative anaerobic taxa, consistent with the early presence of complex organic matter. During the TP, the relative abundance of Bacillota significantly increased to 71.1%, indicating strong thermotolerance. In the MP, Bacillota, Pseudomonadota, and Bacteroidota were the dominant bacterial phyla, with relative abundances of 37.2%, 26.3%, and 18.0%, respectively. This suggests a recovery of microbial diversity at this stage, with a broader range of bacterial taxa participating in the later stages of organic matter degradation. Notably, the relative abundance of the extreme thermophilic phylum Deinococcota increased from 0.1% in IP to 4.7% in MP. This dynamic shift not only underscores the phylum's remarkable adaptability to high-temperature environments but also implies its potential central role in key functions such as high-temperature organic matter degradation and oxidative stress resistance [40].

Genus-level community succession displayed significant thermal adaptation traits ($P < 0.05$) throughout the composting process (Fig. 2b and c). During the TP, canonical thermophiles—such as the genera *Bacillus*, *Truepera*, *Thermobifida*, *Caldibacillus*, and *Pseudogracilibacillus*—exhibited rapid enrichment, with their combined relative abundance rising from 5.7% in the IP to 24.3% in the TP. This underscores their high efficiency in degrading complex organic compounds under hyperthermophilic conditions (>80 °C). Changes in the Simpson and Shannon indices further support this observation (Fig. 2d and e), reflecting dynamic community restructuring under environmental selection pressures. Among them, *Bacillus*, *Caldibacillus*, and *Pseudogracilibacillus* all belong to the phylum Bacillota and exhibit strong tolerance to extreme environmental conditions [39]. These genera demonstrate exceptional capabilities in depolymerizing complex macromolecular organic matter under hyperthermophilic conditions. Notably, *Bacillus*, *Caldibacillus*, and *Pseudogracilibacillus* are spore-forming genera that exhibit remarkable extremotolerance, particularly to thermal stress. *Truepera* (phylum Deinococcota) and *Thermobifida* (phylum Actinomycetota) possess broad substrate degradation capabilities and highly efficient thermostable enzyme systems. These traits enable them to withstand radiation, hyperthermia, and oxidative stress, while contributing to ecological balance and carbon cycling in extreme environments. During the MP, the collective abundance of these thermophiles declined to 12.5%, suggesting a shift toward multifunctional microbial consortia involved in maturation and nutrient cycling as the temperature dropped, substrates were depleted, and microenvironmental homeostasis was established [29,41].

Shifts in the functional categories of clusters of orthologous groups (COGs) and KEGG pathways further elucidate the molecular adaptation mechanisms employed by thermophiles under high-temperature conditions (Fig. 2f and g; see the COG functional category definitions in Supplementary Table S1). During the TP and MP, functions related to translation (functional category J), transcription (functional category K), and amino acid metabolism (functional category E) were significantly enriched compared to the IP ($P < 0.01$). In parallel, genes involved in cell wall or membrane biosynthesis (functional category M) and carbon metabolism (functional category G) were upregulated. These changes supported the sustained synthesis of new proteins and coenzymes at elevated temperatures, while simultaneously reinforcing membrane thermal stability and improving energy metabolism efficiency [42]. Conversely, the downregulation of the mobilome category (functional category X) and energy conversion pathways (functional category C) reflects the strategic suppression of horizontal gene transfer and mobile element activity. This likely serves to minimize genomic instability caused by exogenous DNA insertion or gene rearrangements, thereby maintaining chromosomal integrity and the stability of key physiological processes under thermal stress [43]. This strategy also helps optimize cellular resource allocation and enhances the overall survival of the microbial community. Corresponding KEGG pathway analysis revealed significant enrichment in the “Metabolism” and “Environmental Information Processing” pathway categories during the TP and MP ($P < 0.001$), indicating two parallel adaptation strategies: (i) reinforcement of anabolic and stress-resilient metabolic processes to mitigate oxidative and thermal damage, and (ii) enhanced dynamic sensing of temperature, pH, and redox fluctuations to facilitate rapid environmental responses. These functional shifts provide a molecular basis for the precise regulation of thermostable protein folding, membrane lipid remodeling, and antioxidant defense systems [44,45]. Critically, regression analysis between COG and KEGG annotations demonstrated remarkable consistency ($R^2 = 0.98$, $P < 0.0001$, Fig. 2h), confirming that both metagenomic approaches reliably captured the core functional dynamics of HC. This multidimensional evidence establishes a robust foundation for unraveling the mechanisms of thermal homeostasis regulation in extremophilic microbial communities.

3.2. Differences in gene expression and functional contributions of microorganisms at different stages

During HC, microbial communities exhibit adaptive responses characterized by hierarchical functional regulation and precise molecular remodeling. These processes are driven by temperature fluctuations and are accompanied by the activation and dynamic regulation of HSPs. In this study, we systematically examined overall patterns and stage-specific changes in microbial community functions and gene expression during HC. First, we compared KEGG pathway expression between the IP and TP, as well as between the TP and MP. A total of 2223 pathways were downregulated in the TP compared to the IP (Fig. 3a), with 478 of them being significantly downregulated; and 3510 pathways were upregulated, with 103 of them being significantly upregulated. The upregulated pathways were primarily associated with protein folding, including chaperone systems, *HSP70*, and *groEL*, as well as DNA replication and repair. These pronounced changes in gene expression reflect the rapid adaptation of microbial communities to high-temperature environments, suggesting that enzymatic disruptions caused by thermal stress necessitate the prompt activation of protein repair systems to maintain metabolic continuity [46]. Thus, enrichment and activation of HSPs constitute a core strategy for microbial adaptation to extreme environments at this stage. Meanwhile, in the MP, compared to the TP, 1245 pathways were downregulated (six significantly), while 2789 pathways were upregulated (11 significantly) (Fig. 3b). Following high-temperature selection and adaptation, the microbial functional network became more mature and stable, characterized by an efficient thermal adaptation mechanism and chaperone system that supports sustained intracellular metabolic activity accompanied by a marked decline in differential expression.

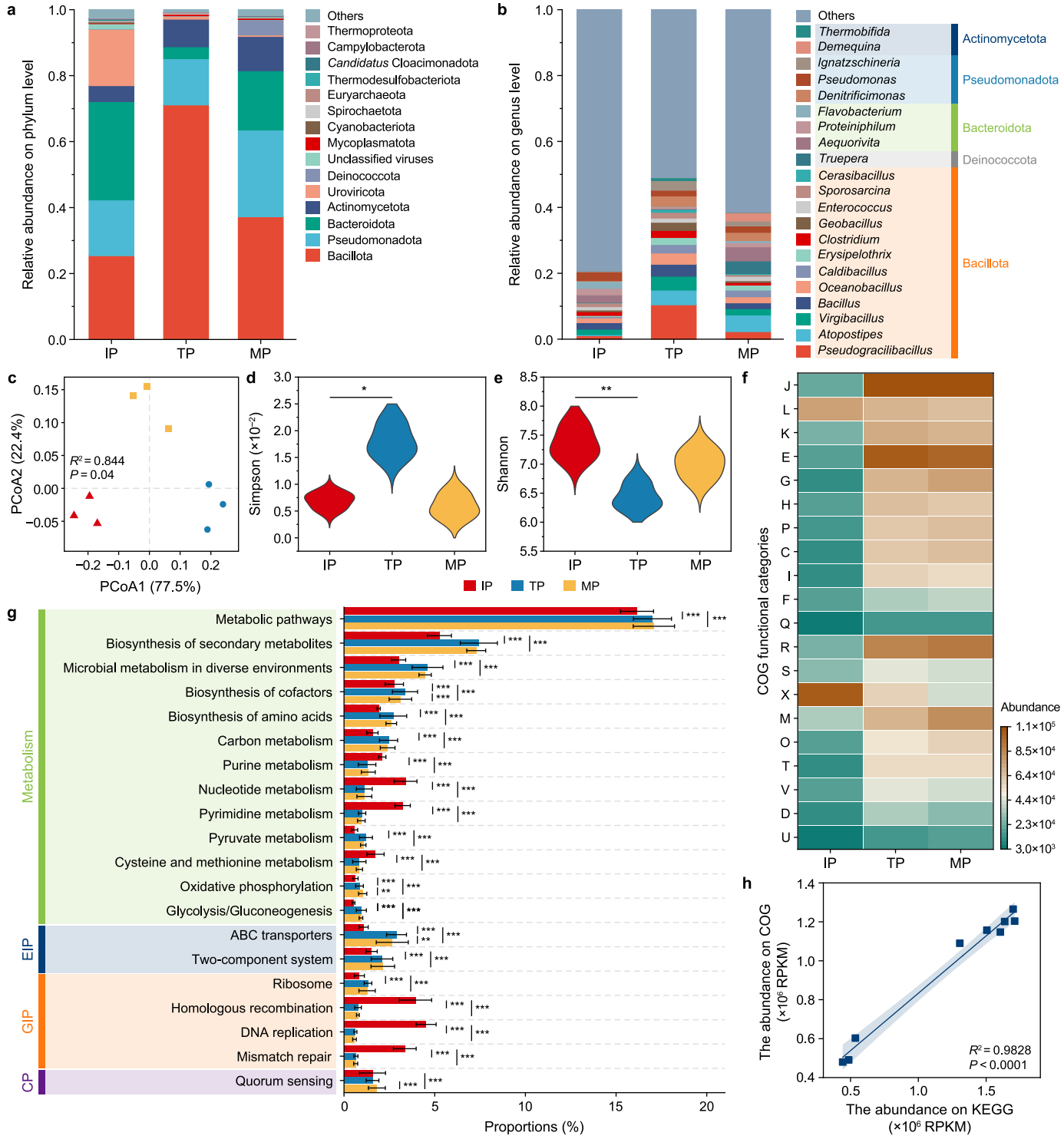

Fig. 2. Community succession and functional metabolic shifts during the hyperthermophilic composting (HC). a, Microbial community composition at the phylum level across different stages of HC. IP: initial phase; TP: thermophilic phase; MP: maturation phase. **b**, Genus-level community composition at each stage, with legend background colors corresponding to phylum-level classifications in panel **a**. **c**, Changes in functional categories of clusters of orthologous groups (COGs) during HC, with functional codes defined in Supplementary Table S1 **d**–**e**, Shannon (**d**) and Simpson (**e**) diversity indices at the genus level across different composting stages, $^{*}P < 0.05$, $^{**}P < 0.01$. **f**, Principal coordinates analysis (PCoA) of β-diversity among samples from different stages of HC. **g**, Differential metabolic pathway profiles at Kyoto encyclopedia of genes and genomes (KEGG) level 3 across composting stages. EIP: environmental information processing; GIP: genetic information processing; CP: cellular processes; $^{***}P < 0.001$. **h**, Correlation analysis between KEGG and COG functional abundances, with shaded regions indicating the 95% confidence interval. RPKM: reads per kilobase per million mapped reads.

To further elucidate the molecular adaptation mechanisms of microbial communities during HC, this study screened heat stress-related genes and focused on the expression of HSPs, such as *dnaK*, *dnaJ*, and *groEL* (Fig. 3c). Compared with the IP, molecular

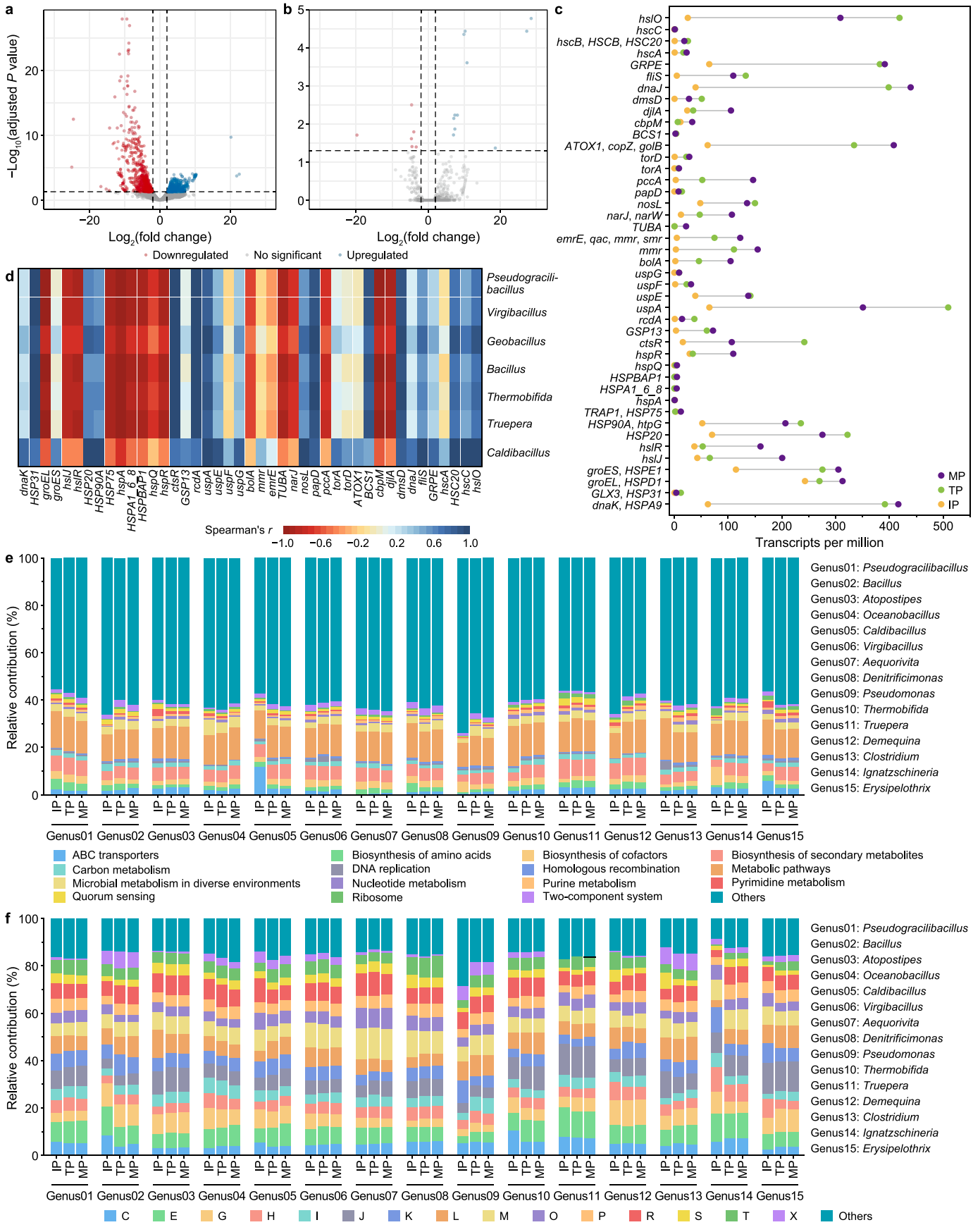
a
b
c
−Log10(adjusted P value)
Log2(fold change)
Downregulated
No significant
Upregulated
hslO
hscC
hscB, HSCB, HSC20
hscA
GRPE
fliS
dnaJ
dmsD
djlA
cbpM
BCS1
ATOX1, copZ, golB
torD
torA
pccA
papD
nosL
narJ, narW
TUBA
emrE, qac, mmr, smr
mmr
bolA
uspG
uspF
uspE
uspA
rcdA
GSP13
ctsR
hspR
hspQ
HSPBAP1
HSPA1_6_8
hspA
TRAP1, HSP75
HSP90A, htpG
HSP20
hslR
hslJ
groES, HSPE1
groEL, HSPD1
GLX3, HSP31
dnaK, HSPA9
MP
TP
IP
Transcripts per million
d
Pseudogracili-bacillus
Virgibacillus
Geobacillus
Bacillus
Thermobifida
Truepera
Caldibacillus
Spearman's r
−1.0 −0.6 −0.2 0.2 0.6 1.0
e
Relative contribution (%)
Genus01: Pseudogracilibacillus
Genus02: Bacillus
Genus03: Atopostipes
Genus04: Oceanobacillus
Genus05: Caldibacillus
Genus06: Virgibacillus
Genus07: Aequorivita
Genus08: Denitrificimonas
Genus09: Pseudomonas
Genus10: Thermobifida
Genus11: Truepera
Genus12: Demequina
Genus13: Clostridium
Genus14: Ignatzschineria
Genus15: Erysipelothrix
IP TP MP
Genus01 Genus02 Genus03 Genus04 Genus05 Genus06 Genus07 Genus08 Genus09 Genus10 Genus11 Genus12 Genus13 Genus14 Genus15
ABC transporters
Carbon metabolism
Microbial metabolism in diverse environments
Quorum sensing
Biosynthesis of amino acids
DNA replication
Nucleotide metabolism
Ribosome
Biosynthesis of cofactors
Homologous recombination
Purine metabolism
Two-component system
Biosynthesis of secondary metabolites
Metabolic pathways
Pyrimidine metabolism
Others
f
Relative contribution (%)
C E G H I J K L M O P R S T X Others

chaperone genes associated with heat stress were significantly upregulated during the TP, reflecting microbial community remodeling at the molecular level to ensure proper protein folding and maintain cellular homeostasis [47]. HSPs serve as frontline defense agents against high-temperature stress, and their enrichment and elevated expression are typically accompanied by disaggregation of protein aggregates and enhanced refolding efficiency. This ensures the continuity of cellular metabolic activity and enables flexible regulation of enzymatic reactions [48]. As the composting process enters the MP, the expression levels of these heat shock-related genes stabilize. This coordinated upregulation across multiple genes and pathways indicates that, under extreme heat stress, various thermophilic bacteria employ a redundant and complementary molecular chaperone network to maintain protein homeostasis and sustain the activity of key metabolic enzymes, thereby ensuring continuous metabolic function [49–51]. Spearman correlation analysis between thermophilic bacteria and heat stress-related genes further supports this conclusion (Fig. 3d). Representative thermophilic genera—such as *Truepera*, *Thermobifida*, and *Bacillus*—exhibited significant positive correlations with key heat shock genes (e.g., *dnaK*, *HSP20*, *HSP90A*, *dnaJ*, and *grpE*; $P < 0.05$; detailed P values are presented in Supplementary Table S2), suggesting that they employ a shared molecular chaperone system to maintain cellular homeostasis during the TP of composting. Notably, compared with the aforementioned genera, *Caldibacillus* exhibited generally higher correlation coefficients with these heat stress genes, suggesting that it may possess more efficient or specialized synergistic mechanisms.

This study illustrates the relative contributions of KEGG metabolic functions by the 15 most dominant bacterial genera (Fig. 3e). Analysis of KEGG level 3 pathway contributions revealed distinct functional partitioning among these dominant genera, associated with thermal adaptation. In typical thermophilic genera, such as *Truepera* and *Thermobifida*, core metabolic pathways and the biosynthesis of secondary metabolites contribute significantly. Additionally, pathways related to adenosine triphosphate (ATP)-binding cassette transporters (ABC transporters), amino acid biosynthesis, and quorum sensing were relatively enriched, suggesting that these genera can rapidly adjust cellular metabolism under extreme thermal conditions by efficiently importing nutrients, exporting toxic byproducts, and sensing environmental fluctuations [52]. Divergent COG functional profiles further delineate genus-specific thermotolerance strategies (Fig. 3f). All dominant genera exhibited elevated representations of COG functional category E (amino acid transport and metabolism) and functional category J (translation and ribosomal biogenesis), with *Truepera* and *Thermobifida* showing particularly strong enrichment. This suggests enhanced ribosomal assembly and translational efficiency, coupled with reinforced amino acid metabolism, to support proper protein folding under thermal stress [53]. These conserved and divergent functional signatures elucidate the molecular basis of thermophilic consortia coevolution during HC, highlighting the pivotal role of HSPs in microbial thermotolerance.

3.3. Thermodynamically driven functional network assembly and microbial cooperation mechanisms in HC

This study correlates composting temperature with specific microbial functions and elucidates their associations with thermophilic bacteria, revealing microbial thermal adaptation mechanisms ranging from macrolevel metabolic pathways to microlevel molecular processes. The co-occurrence network (Fig. 4a) integrates nodes representing temperature, KEGG level 3 pathways, and COG numbers, which are categorized into four functional groups: metabolism, cellular processes, environmental response, and genetic information processing. The network exhibits a high average clustering coefficient of 0.985, indicating dense interconnections within each functional group and strong modularity.

Statistical analysis revealed positive correlations in 86.1%, 66.3%, and 56.4% of KEGG–KEGG, COG–COG, and KEGG–COG interactions, respectively. Notably, 88.2% of KEGG nodes and 92.0% of COG nodes were positively correlated with temperature (Fig. 4b). Additionally, clear coupling and division-of-labor relationships were observed among different functional modules. Among the positively correlated intermodule interactions, 60.6% occurred between metabolism and environmental response, 58.4% between metabolism and genetic information processing, and 53.4% between environmental response and genetic information processing (Fig. 4c). These findings suggest that as pile temperature rises, most functional genes are synchronously upregulated, forming a positively correlated and synergistic network. To further investigate the drivers behind these functional shifts, we performed correlation analyses between the three major modules and both temperature and the abundance of thermophilic bacteria (Fig. 4d–i). Spearman correlation analyses between temperature and the three major modules—metabolism, environmental response, and genetic information processing—further support this trend (Fig. 4d–f, and h).

Additionally, functional modules are not isolated under HC conditions; rather, they form an interconnected, temperature-driven network that ensures energy and substrate supply, activates membrane repair and defense mechanisms, and maintains genomic and protein homeostasis, thereby enabling multilevel thermal adaptation [46]. Additionally, approximately 40.0% of the negative correlations suggest that the microbial community adjusts its functional priorities and makes trade-offs under extreme thermal stress, depending on environmental or resource constraints.

Notably, the synergistic coevolution of functional modules is particularly evident within the network. KEGG pathways that are significantly positively correlated with temperature are primarily involved in core metabolic and repair functions, including cofactor biosynthesis, ABC transporters, and DNA repair pathways such as homologous recombination and mismatch repair. These findings suggest that high temperatures drive microorganisms to enhance energy metabolism and activate repair systems to preserve metabolic and genomic stability. The corresponding COG functional proteins further clarify molecular-level heat tolerance mechanisms. For example, glucose transporter protein (COG2814) and ABC transporters (COG1131) synergistically ensure energy supply and substrate uptake to support efficient carbon metabolism under high temperatures [54]. Site-specific recombinases (COG1961) and DNA-binding proteins (COG0629) safeguard genomic integrity by rapidly repairing DNA double-strand breaks and modulating supercoiled DNA structures [55]. Ribosomal protein (COG0456) and arginine–tRNA synthetase (COG0013) ensure

Fig. 3. Functional contributions and gene expression variations in microbial communities. **a**, Differential KEGG metabolic pathways between the IP and the TP. Significantly downregulated pathways ($\log_2$(fold change) < −1, Adjusted P value < 0.05) are marked in red, upregulated pathways ($\log_2$(fold change) > 1, Adjusted P value < 0.05) in blue, and non-significant pathways in gray. **b**, Differential KEGG metabolic pathways between TP and the MP. IP: initial phase; TP: thermophilic phase; MP: maturation phase. **c**, Lollipop plot of expression levels of selected heat stress-related genes. **d**, Spearman correlation between dominant thermophilic bacteria and heat stress genes. **e–f**, Functional contributions of the top 15 dominant communities at KEGG level 3 (**e**) and COG functional categories (**f**).

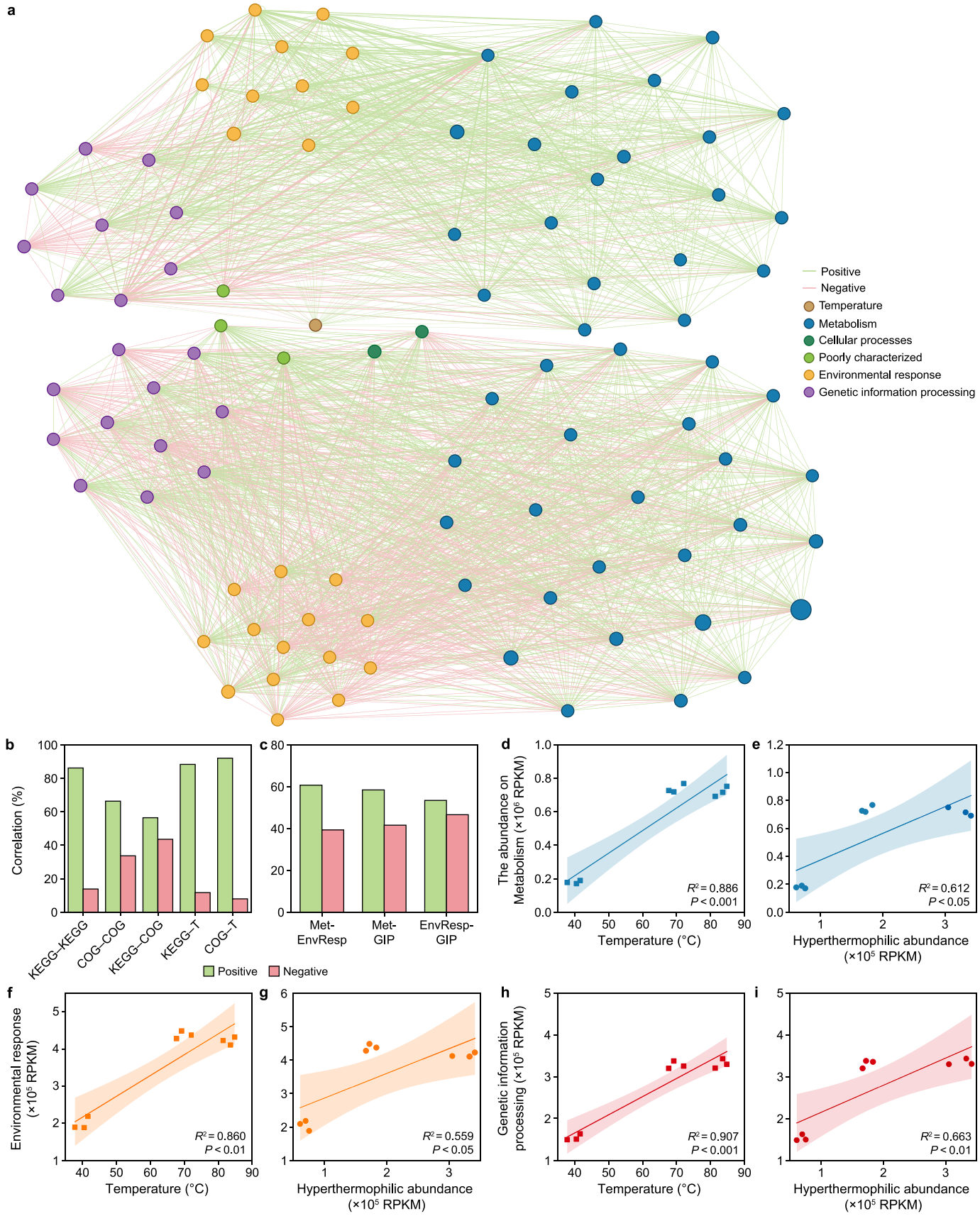

Fig. 4. **a**, Co-occurrence network of metabolic functions and temperature, where green lines indicate positive correlations and pink lines indicate negative correlations. **b**–**g**, The correlations of metabolism (**b**, **c**), environmental response (**d**, **e**), and genetic information processing (**f**, **g**) with temperature (**b**, **d**, **f**) and thermophilic bacterial abundance (**c**, **e**, **g**), the shaded area represents the 95% confidence interval. **h**–**i**, The proportion of positive and negative correlations among interactions within (**h**) and between (**i**) functional modules in the co-occurrence network. T: temperature; GIP: genetic information processing. RPKM: reads per kilobase per million mapped reads.

translational fidelity, thereby preventing protein synthesis errors induced by thermal stress [56]. The coupling of these COGs with KEGG pathways confirms that microorganisms in hyperthermophilic environments prioritize allocating limited energy and resources to sustaining core metabolism and synthesizing essential proteins. This synergistic efficiency is directly reflected in the strong correlation between COG and KEGG abundance changes ($R^2 = 0.98$, $P < 0.0001$; Fig. 2h).

Furthermore, correlation analysis between the three major functional modules—Metabolism, Environmental Response, and Genetic Information Processing—and the abundance of thermophilic bacteria (Fig. 4e–g, and i) revealed significant positive correlations in all cases ($P < 0.05$). The highest R^2 values were observed for the Metabolism and Environmental Response modules, indicating that these functional categories are most strongly associated with shifts in the microbial community. In other words, rising temperatures drive tight coupling and coevolution among functional modules during community succession. Thermophilic bacteria, as functional executors, adapt to and sustain extremely high-temperature environments by enhancing energy metabolism, stabilizing genetic information, and activating stress response pathways, thereby ensuring both system stability and efficient organic degradation under thermal stress. The functional roles and adaptive strategies of dominant thermophilic bacteria further support these proposed mechanisms.

3.4. Potential mechanisms affecting the thermal stability of thermophilic bacteria

To clarify the potential relationships among variables, PLS–PM was used to assess the direct and indirect effects of temperature and key functional modules on microbial heat tolerance mechanisms. In this model, temperature, environmental response, genetic information processing, metabolism, and HSP functional genes were defined as latent variables, while thermophilic bacterial abundance was used as the response variable to represent microbial heat tolerance (Fig. 5a). The PLS–PM model yielded a goodness-of-fit value of 0.851, indicating strong model reliability and explanatory power. The five latent variables collectively explained 97.4% of the variation in thermophilic bacterial abundance, indicating that temperature is the primary driver of heat resistance in HC.

Temperature not only exerted the strongest direct effect on thermophilic bacterial abundance (path coefficient = 0.714) but also indirectly influenced community structure by significantly activating the environmental response (0.848), genetic information processing (0.919), and metabolism (0.632) modules. Among these, genetic information processing exerted a direct effect (0.456) on thermophilic bacterial abundance, suggesting that preserving genomic stability and repair capacity under thermal stress supports the proliferation of thermophilic microbes. In contrast, the negative effect of metabolism (−0.364) implies that basal carbon flux may impose an energetic burden under extreme heat stress.

Notably, HSP functional genes serve as key intermediary nodes, positively regulated by temperature (0.509) and environmental response (0.372). They directly promote the proliferation of thermophilic bacteria (0.522) and partially mitigate the metabolic burden (0.318). The total indirect effect of temperature across multiple pathways was 0.205 (Fig. 5b), further confirming its central regulatory role. The weak negative effect of the environmental response module on thermophilic bacteria (−0.376) was counterbalanced by the positive regulation of HSP genes, highlighting the finely tuned allocation of thermal defense resources within the microbial community [57].

Ultimately, this model elucidates that temperature governs heat resistance through a three-tiered mechanism: directly stimulating microbial proliferation, enhancing genetic stability, and activating HSP-mediated protein protection. HSP genes function as a central hub, integrating environmental cues and metabolic demands to sustain microbial resilience.

The study further validated the diverse adaptive strategies underlying microbial heat tolerance under ultrahigh-temperature conditions using Boruta random forest screening and Mantel correlation analysis. Boruta-based feature importance analysis (Fig. 5c) identified mismatch repair, HSP molecular chaperones (HSP90A and HSP20), and key COG functions—translation initiation (COG functional category K), amino acid metabolism (COG functional category E), and coenzyme transport (COG functional category H)—as the most predictive indicators of microbial heat resistance. These findings underscore the central role of protein quality control in microbial survival under thermal stress—a conclusion further supported by Mantel correlation analysis (Fig. 5d).

However, homologous recombination, DNA replication, mismatch repair, and related functions exhibited systematic negative correlations (Pearson's $r < 0$), suggesting a dynamic reallocation of cellular resources under extreme thermal stress. When temperatures exceed the functional thresholds of DNA repair enzymes, cells redirect limited resources toward immediate protein protection mediated by HSPs and the maintenance of core metabolic processes, thereby ensuring the stability and functional resilience of microbial communities under extreme thermal conditions [58].

3.5. Molecular dynamics insights into the thermal stability mechanisms of key enzymes in thermophiles

While thermophiles are renowned for their resilience to extreme conditions such as radiation and elevated temperatures, the molecular mechanisms underlying their thermal adaptability remain incompletely understood. To investigate this, we selected *T. radiovictrix*—a thermophilic bacterium that exhibits high relative abundance during composting—as the model organism. We focused on three of its key enzymes: DNA polymerase A (DNApolA), ATP synthase subunit α (ATPase_α), and cytidine triphosphate synthase (CTPase), which are not only highly expressed during composting but also play central roles in genetic maintenance and energy metabolism.

To elucidate the structural basis of thermal adaptation, MD simulations of these proteins were performed at 360 K. This study summarizes the simulation outcomes and key thermodynamic parameters for *T. radiovictrix* DNApolA (Fig. 6a). Remarkably, DNApolA exhibited limited conformational disruption under heat stress, with only localized unwinding observed in certain α-helical regions. The RMSD remained stable throughout the trajectory (Supplementary Fig. S1), indicating that the global conformation of DNApolA was largely preserved at high temperatures. RMSF analysis revealed minimal residue-level fluctuations, except in flexible loop regions, suggesting that the core catalytic domains retained high structural rigidity.

The number of intramolecular hydrogen bonds fluctuated slightly but remained consistently elevated, highlighting the critical role of hydrogen bonding in stabilizing DNApolA's secondary and tertiary structures. Moreover, reductions in both the total SASA and the SASA of hydrophobic residues were observed, implying that the protein may mitigate heat-induced denaturation by shielding hydrophobic residues through structural compaction [59]. The Rg stabilized at approximately 3 nm following the initial equilibration phase. While minor fluctuations along the *x*-axis

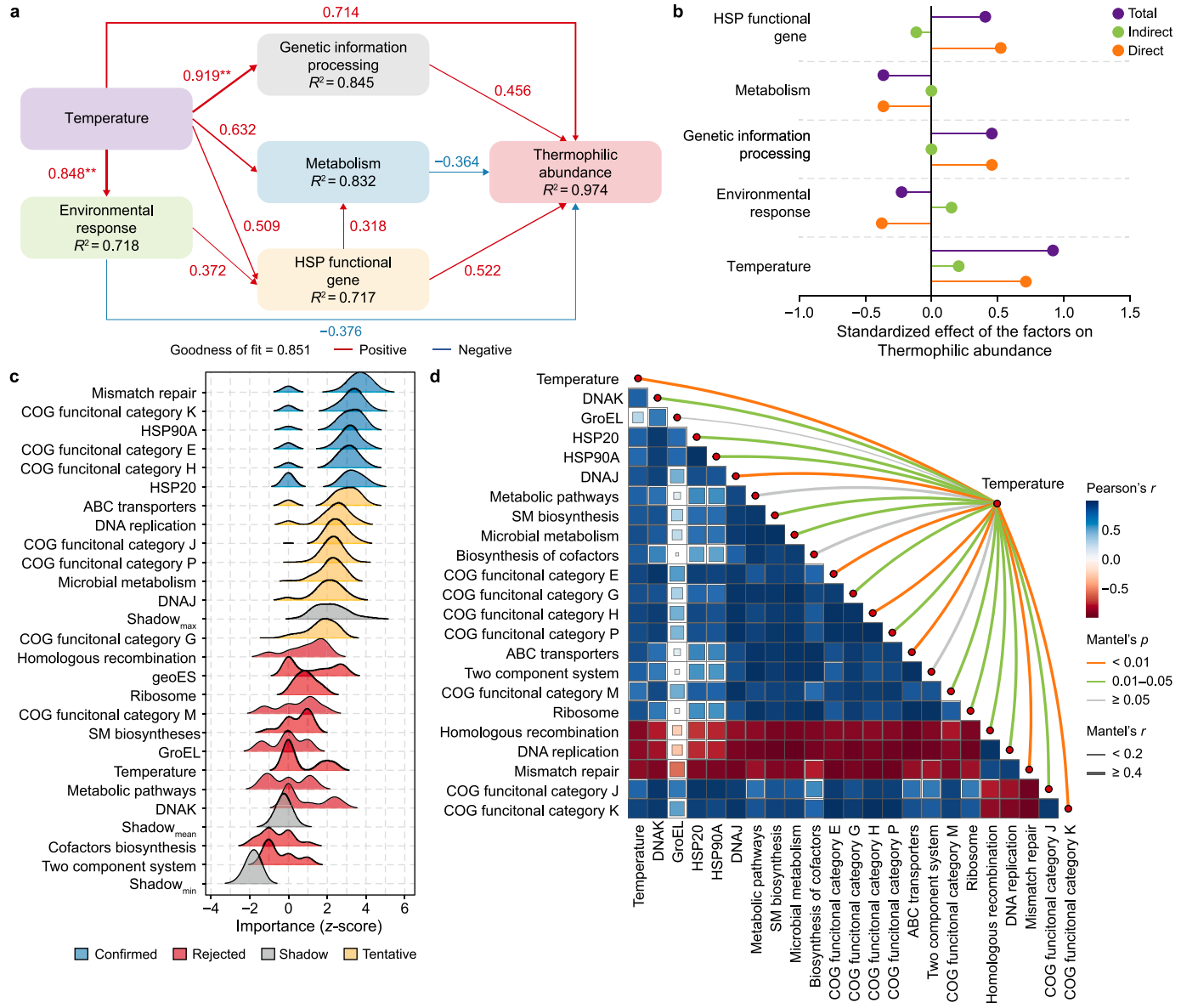

Fig. 5. a, Partial least squares path model (PLS–PM) of thermophile thermotolerance. Arrows show standardized path coefficients (red, negative; blue, positive). The model explains the relationships among temperature, environmental responses, genetic information processing, metabolism, heat shock protein (HSP) functional genes, and thermophile abundance (goodness-of-fit = 0.851). $^{**}P < 0.01$. **b**, Standardized effects on thermophiles abundance derived from PLS–PM analysis. **c**, Boruta random forest analysis identifying key variables influencing thermophiles' abundance. ABC transporters: adenosine triphosphate-binding cassette transporters. **d**, Correlation analysis between temperature, functional modules, and heat stress-related genes.

suggested localized flexibility, the consistent Rg along the *y*- and *z*-axes indicated a tightly packed and structurally rigid core.

Collectively, these findings suggest that *T. radiovictrix* DNApolA achieves thermostability through a combination of compact folding, stable hydrogen bond networks, and reduced solvent exposure of hydrophobic surfaces.

As an extremophile adapted to high-temperature environments, *T. radiovictrix* relies heavily on V-type ATP synthase—particularly V-ATPase_α—as a central component of its energy metabolism machinery. This subunit plays a pivotal role in catalyzing ATP synthesis, a process essential for sustaining cellular function under thermal stress [60]. ATPase_α demonstrated exceptional structural resilience during the MD simulations conducted at 360 K (Fig. 6b). The RMSD remained consistently low throughout the trajectory (Supplementary Fig. S1), indicating minimal global conformational drift and strong preservation of the tertiary structure. Stable hydrogen bond counts and sustained secondary structure elements throughout the simulation further emphasized the thermal robustness of this enzyme, reflecting its ability to retain functional integrity in extreme conditions. RMSF analysis revealed low overall flexibility, with pronounced fluctuations restricted to noncore loop regions, suggesting that the catalytic and structural domains maintain high rigidity. The Rg and SASA metrics remained steady, with no signs of thermally induced expansion or compaction, confirming that the protein preserved its compact folded architecture. Collectively, these results underscore the exceptional thermostability of ATPase_α and highlight its indispensable role in preserving ATP production and cellular energy balance under ultrahigh-temperature conditions.

Although V-ATPase_α is generally stable, partial unwinding of

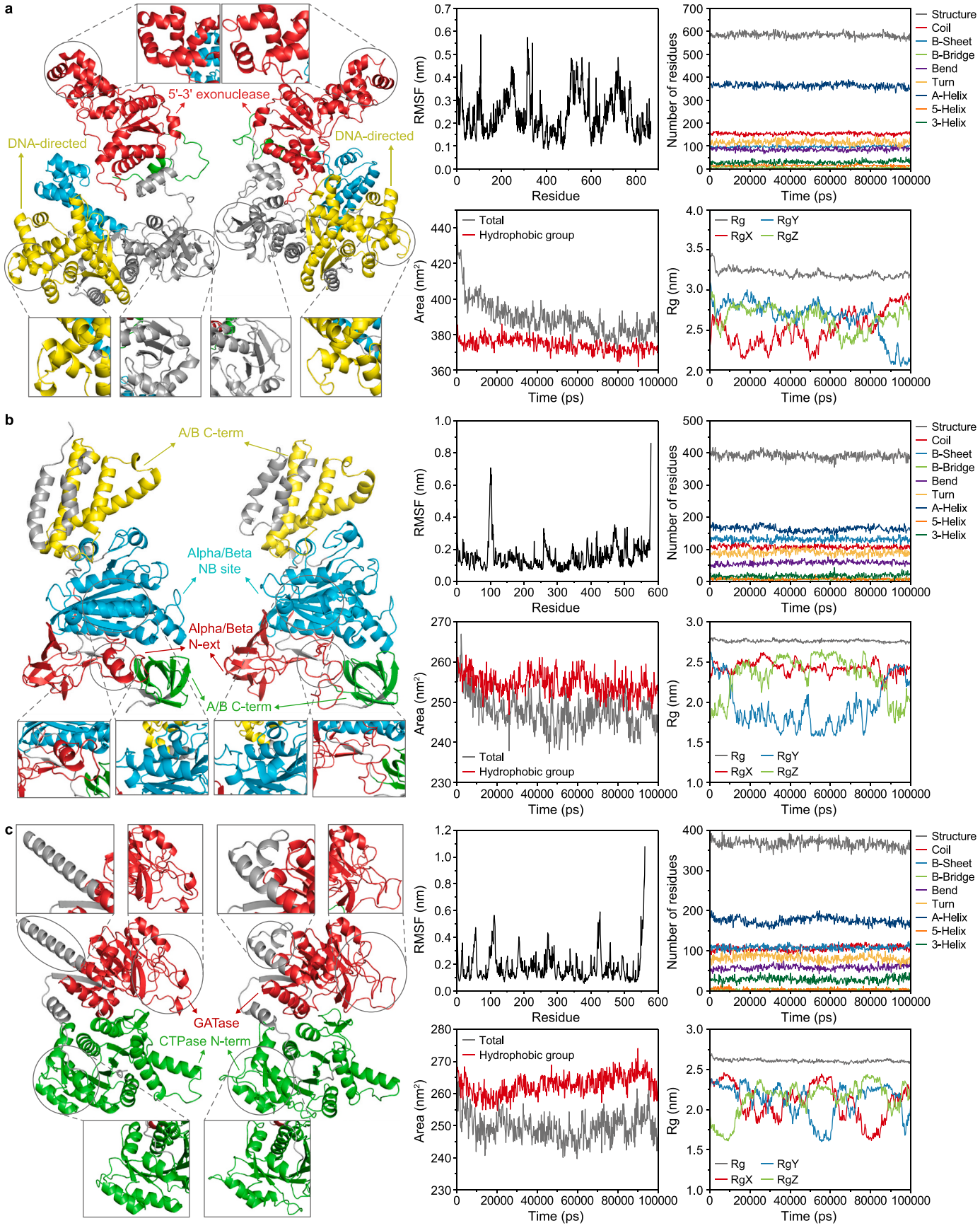

Fig. 6. Stability of key enzymes of *Truepera radiovictrix* at elevated temperatures. Dynamic changes in the protein conformation of DNApolA (**a**), ATPase_α (**b**), and CTPase (**c**) at 360 K. Left: structures before heat-stress simulation; right: structures after simulation. RMSF: root mean square fluctuation; Rg: radius of gyration.

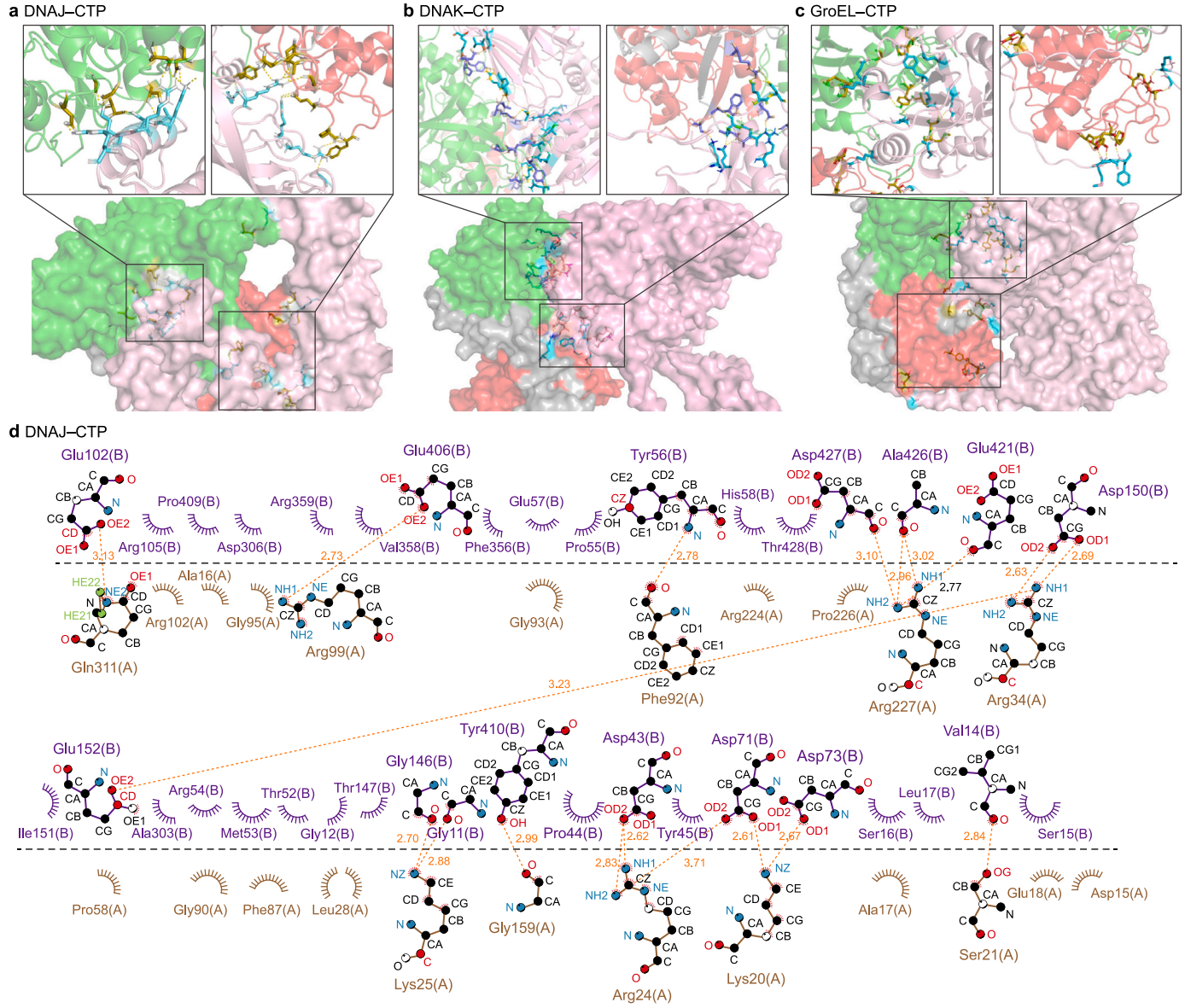

Fig. 7. Molecular repair mechanisms of heat shock proteins on CTPase. a–c, DNAJ (**a**), DANK (**b**), and GroEL (**c**) binding sites on CTP synthase. Pink: DNAJ/DNAK/GroEL; green: N-terminal domain; red: glutamine amidotransferase domain. **d–f**, Detailed interaction patterns between DNAJ (**d**), DNAK (**e**), GroEL (**f**) with CTP synthase, showing binding sites and molecular docking mechanisms.

the localized α-helix occurs within its nucleotide-binding domain and N-terminal extension region. The relevant amino acid residues involved in this unwinding are mainly Arginine (Arg), Glutamic (Glu), Valine (Val), Proline (Pro), Leucine (Leu), Phenylalanine (Phe), and Methionine (Met). Among them, Pro has a rigid ring structure that restricts the flexibility of the backbone and disrupts the hydrogen bond pattern, making the helix more susceptible to loosening under thermal stress. Additionally, the combination of the helix-destabilizing residues Pro and Glycine (Gly) with the hydrogen bond-forming residues Glutamine (Gln) and Serine (Ser) generates a region that is more sensitive to thermal fluctuations [61]. Meanwhile, thermal motion further intensifies atomic vibrations, weakening hydrophobic interactions between residues such as Val, Leu, Phe, and Met. This reduction in hydrophobic stabilization contributes to localized structural instability under thermal stress.

As CTPase is a key enzyme in nucleotide metabolism, maintaining its structural stability and function under high-temperature conditions is crucial for cell survival. Despite minor local adjustments, its overall conformation remained relatively stable at 360 K (Fig. 6c). This observation is further supported by the consistent RMSD trajectory, hydrogen bond count, and secondary structure changes throughout the simulation. The RMSF fluctuated more stably, except for a few isolated residues, and the Rg exhibited large fluctuations along the *y*- and *z*-axes, reflecting increased protein flexibility in certain directions that may facilitate adaptation to dynamic perturbations induced by high temperature. Notably, the SASA of hydrophobic amino acids in CTPase showed a significant upward trend, which may contribute to incorrect protein interactions.

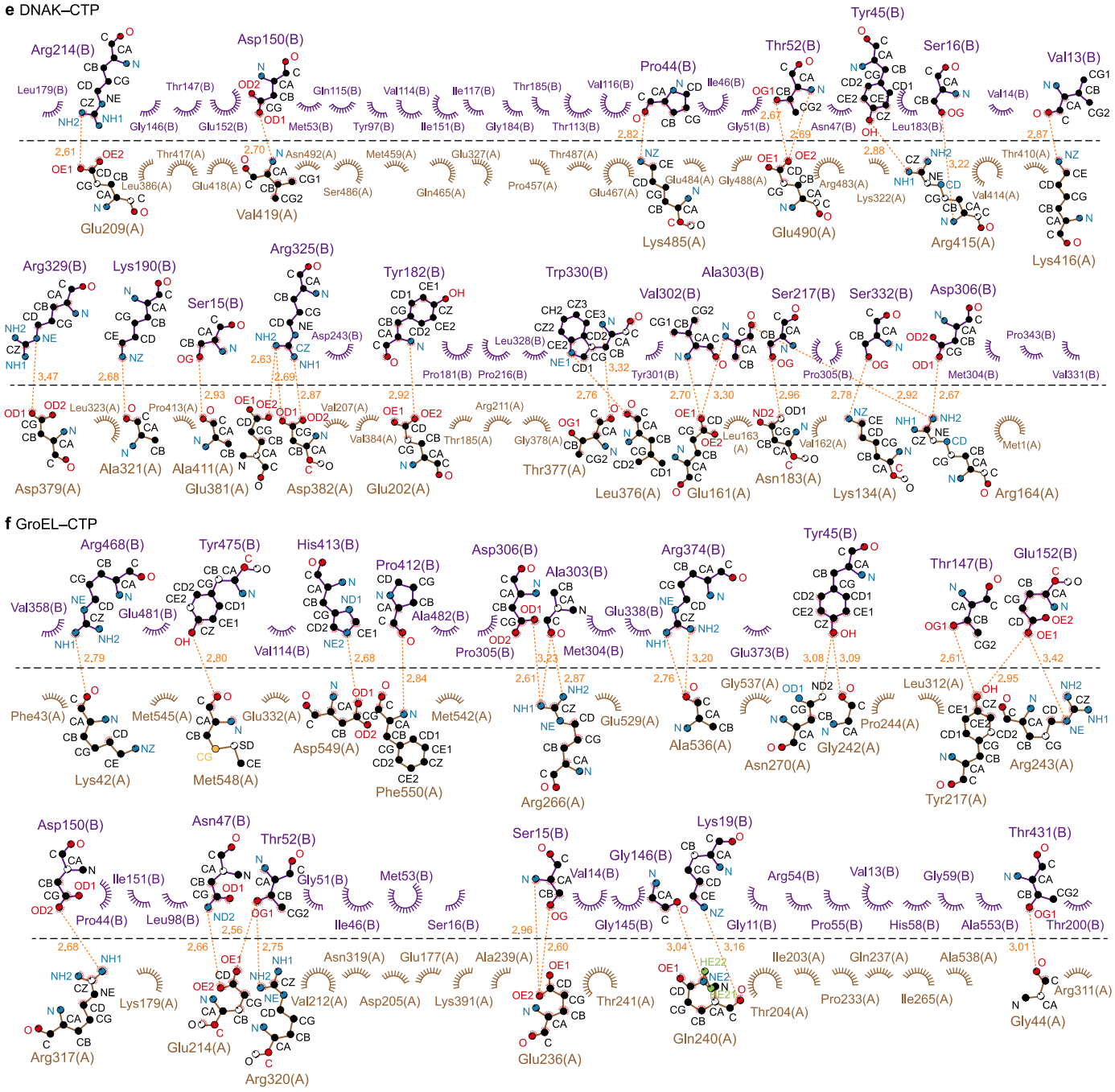

Fig. 7. (*continued*).

3.6. Molecular chaperone-mediated protein repair mechanisms under heat stress in thermophiles

As demonstrated in the previous section, the hydrophobic groups of CTPase were significantly exposed under high-temperature conditions. At this moment, thermophiles typically increase their thermal stability by forming salt bridges or tightening hydrophobic cores. However, at extreme temperatures, regions such as flexible loops and the N/C termini can still undergo loosening or conformational changes; these regions often serve as "hot spots" where molecular chaperones such as DNAK, DNAJ, and GroEL recognize and bind.

To investigate the molecular repair mechanisms employed by *T. radiovictrix* under heat stress, we performed protein docking between molecular chaperones and CTPase (Fig. 7a–c). The functional region of DNAJ binds to the unfolding region of CTPase, and the amino acids in the key binding site include Arg, Gln, Lysine (Lys), Glu, Aspartic (Asp), and Gly (Fig. 7a–d). Among them, the binding of Arg99 and Glu406 forms an ion pair, and the interactions between the polar amino acids facilitate sustained close contact between DNAJ and the target protein, ensuring effective recognition and repair of misfolded proteins [62–64].

Hydrogen-bonded interactions between Arg227, Asp427, alanine (Ala) 426, and Glu421—particularly between Arg227 and multiple acidic amino acids—form a stable charge network that accelerates the folding of the target protein [65]. The

hydrophobic contacts typically formed by the interaction between the aromatic amino acids Phe92 and tyrosine (Tyr) 56 stabilize the target protein, preventing its misfolding or aggregation [66]. Through this stabilization, DNAJ exposes the hydrophobic regions of the target protein, enabling DNAK to bind to them and initiate the correct folding process.

Glu209 and Arg214 are key sites for initiating DNAK's ATP hydrolysis cycle (Fig. 7b–e), and they contribute to the stabilization of the protein–chaperone complex through hydrogen bonding or ion-pair binding [67]. Arg415 forms hydrogen bonds with Tyr45 and Ser16, promoting stable binding of DNAK to the hydrophobic region of the target protein. The Lys416 and Val13 binding sites reinforce this binding by strengthening the hydrophobic region to prevent unwanted aggregation of misfolded proteins with other molecules. Additionally, hydrogen bonding and binding of hydrophobic residues—such as Glu161, Val302, Ala303, Asn183, and Ser217—ensure the target protein's gradual return to its correct folding state by modulating its 3D structure [68].

At these binding sites, DNAK establishes strong contact with the target protein, stabilizing it and preventing it from unfolding at high temperatures through the ATP hydrolysis cycle. The presence of hydrophobic and charged residues at the binding sites further enhances the structural stability of the target protein under high-temperature conditions.

GroEL provides an ideal folding environment for target proteins through its internal cavity and hydrophobic interactions, thereby facilitating the proteins' proper final folding [68]. Docking studies have revealed that GroEL enhances its recognition and binding to target proteins via the electrostatic interactions of Lys42 and Arg468 (Fig. 7c–f), enabling the proteins to smoothly enter its cavity [65]. This process not only stabilizes the protein–chaperone complex through electrostatic forces but also supports the final folding and repair of the target proteins within GroEL.

Moreover, GroEL's mechanism is not solely dependent on its charge network; interactions among hydrophobic residues, such as Met548, Tyr475, and Phe550, form a tighter stabilization zone that prevents the misfolding or aggregation of the target proteins [69]. Additionally, the amino and carboxyl groups of Asn270 can form hydrogen bonds with the hydroxyl group of Tyr45, while the polar side chain of Gly242 can establish hydrogen bonds with oxygen or nitrogen atoms in either Asn270 or Tyr45. These hydrogen bond networks stabilize local structures, reduce the formation of disordered intermediates, accelerate protein folding, and promote correct repair within the GroEL environment [65,66].

4. Conclusion

Our findings offer new insights into microbial adaptation strategies during HC. Rapid temperature elevation accelerated organic matter decomposition, stabilized HSs, and improved nutrient retention efficiency. Microbial succession was characterized by an initial dominance of anaerobes, followed by a shift toward highly thermotolerant *Bacillota*, and a subsequent recovery of community diversity. Functional enrichment in pathways related to metabolism, environmental response, and genetic information processing under heat stress highlighted the importance of maintaining genomic integrity and efficient protein quality control via molecular chaperones. Moreover, integrative network modeling and statistical analyses identified key functional modules and predictive biomarkers associated with thermophilic adaptation.

Under heat stress, microbial communities reprogram their metabolism to prioritize HSP synthesis and reorganization of core metabolic pathways, thereby optimizing energy and resource allocation. Additionally, key proteins in hyperthermophiles exhibit excellent thermal stability. In *Truepera*, protein thermal stability was found to rely not only on intrinsic structural rigidity but also on reduced exposure of hydrophobic regions, optimized amino acid composition, reinforced hydrogen bonds and salt bridge networks, and the synergistic action of molecular chaperone systems. Moreover, hierarchical interactions within the chaperone network were confirmed and elucidated.

Collectively, these findings reveal key thermotolerance mechanisms in thermophilic bacteria and functional streamlining in extreme environments, providing a theoretical foundation for overcoming bottlenecks in composting and enhancing the efficiency of organic matter conversion.

CRediT authorship contribution statement

Xu Li: Writing - Original Draft, Validation, Software, Formal Analysis, Data Curation, Conceptualization. **Youzhao Wang:** Writing - Review & Editing, Visualization, Software, Methodology. **Feng Ma:** Visualization, Data Curation. **Chaoyue Zhao:** Validation, Data Curation. **Yanping Zhang:** Visualization, Data Curation. **Yaonan Zhu:** Supervision, Software, Resources. **Yang Zhang:** Supervision, Software, Resources. **Shujie Hou:** Supervision, Software, Resources. **Bingzhen Li:** Supervision, Software, Resources. **Fuxin Yang:** Supervision, Software, Resources. **Liying Hao:** Writing - Review & Editing, Supervision, Investigation, Funding Acquisition. **Tong Zhu:** Writing - Review & Editing, Supervision, Project Administration, Funding Acquisition.

Declaration of competing interest

The authors declare that they have no known competing financial interests or personal relationships that could have appeared to influence the work reported in this paper.

Acknowledgements

This work was supported by the National Key Research and Development Program of China (No. 2020YFC1806402), the Shenyang Science and Technology Plan Project (No. 20-202-4-37).

Appendix A. Supplementary data

Supplementary data to this article can be found online at https://doi.org/10.1016/j.ese.2025.100630.

Data availability

The sequencing data generated in this study have been deposited in the National Center for Biotechnology Information Sequence Read Archive database (https://www.ncbi.nlm.nih.gov/sra) under accession code PRJNA1216936. Source data are provided in this paper.

References

[1] C. Vieille, G.J. Zeikus, Hyperthermophilic enzymes: sources, uses, and molecular mechanisms for thermostability, Microbiol. Mol. Biol. Rev. 65 (1) (2001) 1–43, https://doi.org/10.1128/mmbr.65.1.1-43.2001.
[2] M.S. Eram, K. Ma, Decarboxylation of pyruvate to acetaldehyde for ethanol production by hyperthermophiles, Biomolecules 3 (3) (2013) 578–596, https://doi.org/10.3390/biom3030578.
[3] M. Dumina, A. Zhgun, Thermo-L-Asparaginases: from the role in the viability of thermophiles and hyperthermophiles at high temperatures to a molecular understanding of their thermoactivity and thermostability, Int. J. Mol. Sci. 24 (3) (2023) 2674, https://doi.org/10.3390/ijms24032674.
[4] M.S. Urbieta, E.R. Donati, K.G. Chan, S. Shahar, L.L. Sin, K.M. Goh, Thermophiles in the genomic era: biodiversity, science, and applications, Biotechnol. Adv. 33 (6) (2015) 633–647, https://doi.org/10.1016/j.

biotechadv.2015.04.007.
[5] H. Jung, Y. Inaba, S. Banta, Genetic engineering of the acidophilic chemolithoautotroph Acidithiobacillus ferrooxidans, Trends Biotechnol. 40 (6) (2022) 677–692, https://doi.org/10.1016/j.tibtech.2021.10.004.
[6] J. Chen, Y. Liu, P. Diep, R. Mahadevan, Genetic engineering of extremely acidophilic Acidithiobacillus species for biomining: progress and perspectives, J. Hazard. Mater. 438 (2022) 129456, https://doi.org/10.1016/j.jhazmat.2022.129456.
[7] N. Pradhan, L. Dipasquale, G. d'Ippolito, A. Panico, P.N.L. Lens, G. Esposito, A. Fontana, Hydrogen and lactic acid synthesis by the wild-type and a laboratory strain of the hyperthermophilic bacterium Thermotoga neapolitana DSMZ 4359T under capnophilic lactic fermentation conditions, Int. J. Hydrogen Energy 42 (25) (2017) 16023–16030, https://doi.org/10.1016/j.ijhydene.2017.05.052.
[8] I. Orita, R. Futatsuishi, K. Adachi, T. Ohira, A. Kaneko, K. Minowa, M. Suzuki, T. Tamura, S. Nakamura, T. Imanaka, T. Suzuki, T. Fukui, Random mutagenesis of a hyperthermophilic archaeon identified tRNA modifications associated with cellular hyperthermotolerance, Nucleic Acids Res. 47 (4) (2019) 1964–1976, https://doi.org/10.1093/nar/gky1313.
[9] T. Miyamoto, S. Nitta, H. Homma, S. Fushinobu, Functional and structural analyses of a highly multifunctional enzyme TM1270 from the hyperthermophile Thermotoga maritima, ACS Catal. 14 (24) (2024) 18817–18830, https://doi.org/10.1021/acscatal.4c05275.
[10] K.H. Seistrup, S. Rose, U. Birkedal, H. Nielsen, H. Huber, S. Douthwaite, Bypassing rRNA methylation by RsmA/Dim1during ribosome maturation in the hyperthermophilic archaeon *Nanoarchaeum equitans*, Nucleic Acids Res. 45 (4) (2017) 2007–2015, https://doi.org/10.1093/nar/gkw839.
[11] T. Oshima, T. Moriya, A preliminary analysis of microbial and biochemical properties of high-temperature compost, Ann. N. Y. Acad. Sci. 1125 (2008) 338–344, https://doi.org/10.1196/annals.1419.012.
[12] F. Ma, T. Zhu, S. Yao, H.Y. Quan, K. Zhang, B.R. Liang, Y.Z. Wang, Y.A. Zhu, C. Y. Zhao, Z. Lyu, Coupling effect of high temperature and thermophilic bacteria indirectly accelerates the humification process of municipal sludge in hyperthermophilic composting, Process Saf. Environ. Prot. 166 (2022) 469–477, https://doi.org/10.1016/j.psep.2022.08.052.
[13] H.P. Liao, X.M. Lu, C. Rensing, V.P. Friman, S. Geisen, Z. Chen, Z. Yu, Z. Wei, S. G. Zhou, Y.G. Zhu, Hyperthermophilic composting accelerates the removal of antibiotic resistance genes and Mobile genetic elements in sewage sludge, Environ. Sci. Technol. 52 (1) (2018) 266–276, https://doi.org/10.1021/acs.est.7b04483.
[14] F. Ma, T. Zhu, Y. Wang, S. Torii, Z. Wang, C. Zhao, X. Li, Y. Zhang, H. Quan, C. Yuan, L. Hao, Adsorption mechanism and remediation of heavy metals from soil amended with hyperthermophilic composting products: exploration of waste utilization, Bioresour. Technol. 410 (2024) 131292, https://doi.org/10.1016/j.biortech.2024.131292.
[15] H.P. Liao, C. Liu, C.F. Ai, T. Gao, Q.E. Yang, Z. Yu, S.M. Gao, S.G. Zhou, V. P. Friman, Mesophilic and thermophilic viruses are associated with nutrient cycling during hyperthermophilic composting, ISME J. 17 (6) (2023) 916–930, https://doi.org/10.1038/s41396-023-01404-1.
[16] J.C. Mathai, G.D. Sprott, M.L. Zeidel, Molecular mechanisms of water and solute transport across archaebacterial lipid membranes, J. Biol. Chem. 276 (29) (2001) 27266–27271, https://doi.org/10.1074/jbc.M103265200.
[17] J.D. Trent, A review of acquired thermotolerance, heat-shock proteins, and molecular chaperones in archaea, FEMS Microbiol. Rev. 18 (2–3) (1996) 249–258, https://doi.org/10.1016/0168-6445(96)00016-2.
[18] J. Tyedmers, A. Mogk, B. Bukau, Cellular strategies for controlling protein aggregation, Nat. Rev. Mol. Cell Biol. 11 (11) (2010) 777–788, https://doi.org/10.1038/nrm2993.
[19] M. Roy, K. Bhakta, A. Bhowmick, S. Gupta, A. Ghosh, A. Ghosh, Archaeal Hsp14 drives substrate shuttling between small heat shock proteins and thermosome: insights into a novel substrate transfer pathway, FEBS J. 289 (4) (2022) 1080–1104, https://doi.org/10.1111/febs.16226.
[20] P. Villain, V. Da Cunha, E. Villain, P. Forterre, J. Oberto, R. Catchpole, T. Basta, The hyperthermophilic archaeon *Thermococcus kodakarensis* is resistant to pervasive negative supercoiling activity of DNA gyrase, Nucleic Acids Res. 49 (21) (2021) 12332–12347, https://doi.org/10.1093/nar/gkab869.
[21] M. Brunderová, V. Havlicek, J. Matyasovsky, R. Pohl, L.P. Slavetinská, M. Krömer, M. Hocek, Expedient production of site specifically nucleobase-labelled or hypermodified RNA with engineered thermophilic DNA polymerases, Nat. Commun. 15 (1) (2024) 3054, https://doi.org/10.1038/s41467-024-47444-9.
[22] H. Radianingtyas, P.C. Wright, Alcohol dehydrogenases from thermophilic and hyperthermophilic archaea and bacteria, FEMS Microbiol. Rev. 27 (5) (2003) 593–616, https://doi.org/10.1016/s0168-6445(03)00068-8.
[23] T. Xie, L. Zhou, L. Han, C. You, Z. Liu, W. Cui, Z. Cheng, J. Guo, Z. Zhou, Engineering hyperthermophilic pullulanase to efficiently utilize corn starch for production of maltooligosaccharides and glucose, Food Chem. 446 (2024) 138652, https://doi.org/10.1016/j.foodchem.2024.138652.
[24] J.E. Graham, M.E. Clark, D.C. Nadler, S. Huffer, H.A. Chokhawala, S.E. Rowland, H.W. Blanch, D.S. Clark, F.T. Robb, Identification and characterization of a multidomain hyperthermophilic cellulase from an archaeal enrichment, Nat. Commun. 2 (2011) 375, https://doi.org/10.1038/ncomms1373.
[25] F. Akram, I. ul Haq, A. Aqeel, Z. Ahmed, F.I. Shah, Thermostable cellulases: structure, catalytic mechanisms, directed evolution and industrial implementations, Renew. Sust. Energ. Rev. 151 (2021) 111597, https://doi.org/10.1016/j.rser.2021.111597.
[26] S.F. Chen, Y.Q. Zhou, Y.R. Chen, J. Gu, Fastp: an ultra-fast all-in-one FASTQ preprocessor, Bioinformatics 34 (17) (2018) 884–890, https://doi.org/10.1093/bioinformatics/bty560.
[27] D.H. Li, C.M. Liu, R.B. Luo, K. Sadakane, T.W. Lam, MEGAHIT: an ultra-fast single-node solution for large and complex metagenomics assembly via succinct *de Bruijn* graph, Bioinformatics 31 (10) (2015) 1674–1676, https://doi.org/10.1093/bioinformatics/btv033.
[28] D. Hyatt, G.L. Chen, P.F. LoCascio, M.L. Land, F.W. Larimer, L.J. Hauser, Prodigal: prokaryotic gene recognition and translation initiation site identification, BMC Bioinf. 11 (2010) 119, https://doi.org/10.1186/1471-2105-11-119.
[29] L.M. Fu, B.F. Niu, Z.W. Zhu, S.T. Wu, W.Z. Li, CD-HIT: accelerated for clustering the next-generation sequencing data, Bioinformatics 28 (23) (2012) 3150–3152, https://doi.org/10.1093/bioinformatics/bts565.
[30] R.Q. Li, Y.R. Li, K. Kristiansen, J. Wang, SOAP: short oligonucleotide alignment program, Bioinformatics 24 (5) (2008) 713–714, https://doi.org/10.1093/bioinformatics/btn025.
[31] B. Buchfink, C. Xie, D.H. Huson, Fast and sensitive protein alignment using DIAMOND, Nat. Methods 12 (1) (2015) 59–60, https://doi.org/10.1038/nmeth.3176.
[32] M.J. Abraham, T. Murtola, R. Schulz, S. Páll, J.C. Smith, B. Hess, E. Lindahl, GROMACS: high performance molecular simulations through multi-level parallelism from laptops to supercomputers, SoftwareX 1–2 (2015) 19–25, https://doi.org/10.1016/j.softx.2015.06.001.
[33] J.A.J.L.J.o.C.M.S. Lemkul From proteins to perturbed hamiltonians: a suite of tutorials for the GROMACS-2018 molecular simulation package, Living J. Comput. Mol. Sci. (2019) 5068, https://doi.org/10.33011/LIVECOMS.1.1.5068 [Article v1.0].
[34] R.V. Honorato, M.E. Trellet, B. Jiménez-García, J.J. Schaarschmidt, M. Giulini, V. Reys, P.I. Koukos, J.P.G.L.M. Rodrigues, E. Karaca, G.C.P. van Zundert, J. Roel-Touris, C.W. van Noort, Z. Jandová, A.S.J. Melquiond, A.M.J.J. Bonvin, The HADDOCK2.4 web server for integrative modeling of biomolecular complexes, Nat. Protoc. 19 (11) (2024) 3219–3241, https://doi.org/10.1038/s41596-024-01011-0.
[35] R.V. Honorato, P.I. Koukos, B. Jiménez-García, A. Tsaregorodtsev, M. Verlato, A. Giachetti, A. Rosato, A. Bonvin, Structural biology in the clouds: the WeNMR-EOSC ecosystem, Front. Mol. Neurosci. 8 (2021) 729513, https://doi.org/10.3389/fmolb.2021.729513.
[36] B.T. Liu, K.F. Yu, I. Ahmed, K. Gin, B.D. Xi, Z.M. Wei, Y.L. He, B. Zhang, Key factors driving the fate of antibiotic resistance genes and controlling strategies during aerobic composting of animal manure: a review, Sci. Total Environ. 791 (2021) 148372, https://doi.org/10.1016/j.scitotenv.2021.148372.
[37] Q.Z. Wang, J. Gu, X.J. Wang, J.Y. Ma, T. Hu, H.L. Peng, J.F. Bao, R.R. Zhang, Effects of nano-zerovalent iron on antibiotic resistance genes and mobile genetic elements during swine manure composting, Environ. Pollut. 258 (2020) 113654, https://doi.org/10.1016/j.envpol.2019.113654.
[38] R.Z. Xing, X.G. Yang, H.Y. Sun, X.Y. Ye, H.P. Liao, S.P. Qin, Z. Chen, S.G. Zhou, Extensive production and evolution of free radicals during composting, Bioresour. Technol. 359 (2022) 127491, https://doi.org/10.1016/j.biortech.2022.127491.
[39] C. Zhao, F. Ma, Y. Wang, X. Li, Y. Zhang, Z. Wang, W. Xiong, X. Gao, Y. Ma, F. Yang, T. Zhu, Enhancing humification in high-temperature composting: insights from endogenous and exogenous heating strategies, Bioresour. Technol. 419 (2025) 132099, https://doi.org/10.1016/j.biortech.2025.132099.
[40] Y. He, Y. He, N. Abdullah Al-Dhabi, P. Gao, H. Huang, B. Yan, X. Cui, W. Tang, J. Zhang, Y. Lu, F. Peng, Effects of exogenous thermophilic bacteria and ripening agent on greenhouse gas emissions, enzyme activity and microbial community during straw composting, Bioresour. Technol. 407 (2024) 131114, https://doi.org/10.1016/j.biortech.2024.131114.
[41] S. Zhou, Z. Song, Z. Li, R. Qiao, M. Li, Y. Chen, H. Guo, Mechanisms of nitrogen transformation driven by functional microbes during thermophilic fermentation in an ex situ fermentation system, Bioresour. Technol. 350 (2022) 126917, https://doi.org/10.1016/j.biortech.2022.126917.
[42] Q. Chen, J. Wang, H. Zhang, H. Shi, G. Liu, J. Che, B. Liu, Microbial community and function in nitrogen transformation of ectopic fermentation bed system for pig manure composting, Bioresour. Technol. 319 (2021) 124155, https://doi.org/10.1016/j.biortech.2020.124155.
[43] G. Wang, Y. Kong, Y. Yang, R. Ma, L. Li, G. Li, J. Yuan, Composting temperature directly affects the removal of antibiotic resistance genes and mobile genetic elements in livestock manure, Environ. Pollut. 303 (2022) 119174, https://doi.org/10.1016/j.envpol.2022.119174.
[44] S.H. Chen, J. Gu, S.Y. Zhang, R. Yu, Application of hyperthermophiles in sludge composting: a review, Environmental Chem. Lett. 22 (1) (2024) 445–460, https://doi.org/10.1007/s10311-023-01657-4.
[45] X. Bai, Y. Shi, L. Tang, L. Chen, H. Fan, H. Wang, J. Wang, X. Jia, S. Chen, S. Lai, Heat stress affects faecal microbial and metabolic alterations of rabbits, Front. Microbiol. 12 (2021) 817615, https://doi.org/10.3389/fmicb.2021.817615.
[46] D. Li, H. Wang, J. Ding, Y. Zhou, Y. Jia, S. Fan, A. Zhang, Y. Shen, Comparative study on aerobic compost performance, microbial communities and metabolic functions between human feces and cattle manure composting, Environ. Technol. Innovat. 31 (2023) 103230, https://doi.org/10.1016/j.eti.2023.103230.
[47] N. Peng, J. Zhang, R. Hu, S. Liu, F. Liu, Y. Fan, H. Yang, J. Huang, J. Ding, R. Chen,

L. Li, Z. He, C. Wang, Hidden pathogen risk in mature compost: low optimal growth temperature confers pathogen survival and activity during manure composting, J. Hazard. Mater. 480 (5) (2024) 136230, https://doi.org/10.1016/j.jhazmat.2024.136230.
[48] A. Szabo, T. Langer, H. Schroder, J. Flanagan, B. Bukau, F.U. Hartl, The ATP hydrolysis-dependent reaction cycle of the Escherichia coli Hsp70 system DnaK, DnaJ, and GrpE, Proc. Natl. Acad. Sci. U.S.A 91 (1994) 10345–10349, https://doi.org/10.1073/pnas.91.22.10345.
[49] N. Rosic, J. Delamare-Deboutteville, S. Dove, Heat stress in symbiotic dinoflagellates: implications on oxidative stress and cellular changes, Sci. Total Environ. 944 (2024) 173916, https://doi.org/10.1016/j.scitotenv.2024.173916.
[50] C.K. Mathews, Deoxyribonucleotide metabolism, mutagenesis and cancer, Nat. Rev. Cancer 15 (2015) 528–539, https://doi.org/10.1038/nrc3981.
[51] R.A. Sclafani, T.M. Holzen, Cell cycle regulation of DNA replication, Annu. Rev. Genet. 41 (2007) 237–280, https://doi.org/10.1146/annurev.genet.41.110306.130308.
[52] Y. He, W. Chen, Y. Xiang, Y. Zhang, L. Xie, Unveiling the effect of PFOA presence on the composting process: roles of oxidation stress, carbon metabolism, and humification process, J. Hazard. Mater. 479 (2024) 135682, https://doi.org/10.1016/j.jhazmat.2024.135682.
[53] Z. Wei, T. Ahmed Mohamed, L. Zhao, Z. Zhu, Y. Zhao, J. Wu, Microhabitat drive microbial anabolism to promote carbon sequestration during composting, Bioresour. Technol. 346 (2022) 126577, https://doi.org/10.1016/j.biortech.2021.126577.
[54] S. Gu, Z. Zhao, F. Xue, D. Liu, Q. Liu, J. Li, C. Tian, The arabinose transporter MtLat-1 is involved in hemicellulase repression as a pentose transceptor in Myceliophthora thermophila, Biotechnol. Biofuels Bioprod. 16 (1) (2023) 51, https://doi.org/10.1186/s13068-023-02305-3.
[55] J. Li, J. Wang, S. Ruiz-Cruz, M. Espinosa, J.-R. Zhang, A. Bravo, In vitro DNA inversions mediated by the PsrA site-specific tyrosine recombinase of Streptococcus pneumoniae, Front. Mol. Biosci. 7 (2020) 00043, https://doi.org/10.3389/fmolb.2020.00043.
[56] H. Cui, M. Kapur, J.K. Diedrich, J.R. Yates III, Susan L. Ackerman, P. Schimmel, Regulation of ex-translational activities is the primary function of the multi-tRNA synthetase complex, Nucleic Acids Res. 49 (2020) 3603–3616, https://doi.org/10.1093/nar/gkaa1183.
[57] T. Li, X. Zhang, X. Wang, Z. Yan, C. Peng, S. Zhao, D. Xu, D. Liu, Q. Shen, Effect of inoculating thermophilic bacterial consortia on compost efficiency and quality, Waste Manage. (Tucson, Ariz.) 170 (2023) 341–353, https://doi.org/10.1016/j.wasman.2023.09.023.
[58] M. Mannaa, A. Mansour, I. Park, D.-W. Lee, Y.-S. Seo, Insect-based agri-food waste valorization: agricultural applications and roles of insect gut microbiota, Environ. Sci. Ecotechnol. 17 (2024) 100287, https://doi.org/10.1016/j.ese.2023.100287.
[59] H. Huang, C. Simmerling, Fast pairwise approximation of solvent accessible surface area for implicit solvent simulations of proteins on CPUs and GPUs, J. Chem. Theor. Comput. 14 (11) (2018) 5797–5814, https://doi.org/10.1021/acs.jctc.8b00413.
[60] D. Litty, V. Müller, ATP synthesis in an ancient ATP synthase at low driving forces, P Proc. Natl. Acad. Sci. U.S.A 119 (19) (2022) e2201921119, https://doi.org/10.1073/pnas.2201921119.
[61] S. Gahlawat, J. Siess, N. Losada, J. Timm, V. Nanda, D.I. Shreiber, Impact of vascular Ehlers-Danlos Syndrome-associated Gly substitutions on structure, function, and mechanics using bacterial collagen, Matrix Biol. 135 (2025) 87–98, https://doi.org/10.1016/j.matbio.2024.12.002.
[62] C.L. Wang, H.L. Yang, Conserved residues in the subunit interface of tau Glutathione S-transferase affect catalytic and structural functions, J. Integr. Plant Biol. 53 (1) (2011) 35–43, https://doi.org/10.1111/j.1744-7909.2010.01005.x.
[63] M. Rezaeian, M. Izadyar, M.R. Housaindokht, Exploring the interaction of amino acid-based ionic liquids in water and organic solvents: insight from MD simulations and QM calculations, J. Mol. Liq. 327 (2021) 114867, https://doi.org/10.1016/j.molliq.2020.114867.
[64] F.H. Leinberger, B.A. Berghoff, Relevance of charged and polar amino acids for functionality of membrane toxin TisB, Sci. Rep. 14 (1) (2024) 22998, https://doi.org/10.1038/s41598-024-73879-7.
[65] Y. Lv, S. Luo, K. Huang, H. Wang, S. Dong, Y. Cong, J.Z.H. Zhang, L. Duan, Investigating effects of bridging water on the binding of neuraminidase–ligands using computational alanine scanning combined with interaction entropy method, J. Mol. Liq. 336 (2021) 116214, https://doi.org/10.1016/j.molliq.2021.116214.
[66] F. Qin, B. Qin, T. Mori, Y. Wang, L. Meng, X. Zhang, X. Jia, I. Abe, S. You, Engineering of Candida glabrata ketoreductase 1 for asymmetric reduction of α-Halo ketones, ACS Catal. 6 (9) (2016) 6135–6140, https://doi.org/10.1021/acscatal.6b01552.
[67] R. Kobayashi, H. Ueno, K.-i. Okazaki, H. Noji, Molecular mechanism on forcible ejection of ATPase inhibitory factor 1 from mitochondrial ATP synthase, Nat. Commun. 14 (1) (2023) 1682, https://doi.org/10.1038/s41467-023-37182-9.
[68] M. Paloni, C. Cavallotti, Molecular modeling of the interaction of protein L with antibodies, ACS Omega 2 (10) (2017) 6464–6472, https://doi.org/10.1021/acsomega.7b01123.
[69] D. Chakravarty, S.C. Bihani, M. Banerjee, A. Ballal, Novel molecular insights into the anti-oxidative stress response and structure-function of a salt-inducible cyanobacterial Mn-catalase, Plant Cell Environ. 42 (8) (2019) 2508–2521, https://doi.org/10.1111/pce.13563.